Active normal faulting during the 1997 seismic sequence in Colfiorito, Umbria: Did slip propagate to the surface?

Zoë K. Mildon[1.], Gerald P. Roberts[2.], Joanna P. FAURE WALKER[1.], Luke N. J. Wedmore[1.], Ken J. W. McCaffrey[3.]

1. Institute for Risk and Disaster Reduction, University College London, Gower Street, London, WC1E 6BT

2. Department of Earth and Planetary Sciences, Birkbeck, University of London, Malet Street, London, WC1E 7HX

3. Department of Earth Sciences, Durham University, Durham DH1 3LE

Corresponding author: Z.K. Mildon, Institute for Risk and Disaster Reduction, University College London, Gower Street, London, WC1E 6BT, zoe.mildon.13@ucl.ac.uk

Keywords: mechanics of faulting, tectonic geomorphology, active faulting, coseismic surface slip

Abstract

In order to determine whether slip during an earthquake on the 26th September 1997 propagated to the surface, structural data have been collected along a bedrock fault scarp in Umbria, Italy. These collected data are used to investigate the relationship between the throw associated with a debated surface rupture (observed as a pale unweathered stripe at the base of the bedrock fault scarp) and the strike, dip and slip-vector Previous studies have suggested the surface rupture was produced either by primary surface slip or secondary compaction of hangingwall sediments. Some authors favour the latter because sparse surface fault dip measurements do not match nodal plane dips at depth. It is demonstrated herein that the strike, dip and height of the surface rupture, represented by a pale unweathered stripe at the base of the bedrock scarp, shows a systematic relationship with respect to the geometry and kinematics of faulting in the bedrock. The strike and dip co-vary and the throw is greatest where the strike is oblique to the slip-vector azimuth where the highest dip values are recorded. This implies that the throw values vary to accommodate spatial variation in the strike and dip of the fault across fault plane corrugations, a feature that is predicted by theory describing conservation of strain along faults, but not by compaction. Furthermore, published earthquake locations and reported fault dips are consistent with the analysed surface scarps when natural variation for surface dips and uncertainty for nodal plane dips at depth are taken into account. This implies that the fresh stripe is indeed a primary coseismic surface rupture whose slip is connected to the seismogenic fault at depth. We discuss how this knowledge of the locations and geometry of the active faults can be used as an input for seismic hazard assessment.

1. Introduction

For seismic hazard assessment it is important to know the locations and geometries of active faults, as the proximity of a location to an active fault is a key factor that determines the predicted degree of shaking (e.g. *Roberts et al.*, 2004). There are some examples of seismic hazard assessment in different tectonic settings that use active fault traces as an input for probabilistic seismic hazard assessment (PSHA), notably the Uniform California Earthquake Rupture Forecast (UCERF, *Field et al.*, 2009), as well as PSHA for Taiwan (*Cheng et al.*, 2007) and New Zealand (*Stirling et al.*, 2002). In the central Italian Apennines an ongoing debate concerns the locations of active faults with one key issue being whether earthquake slip at depth propagates to the surface producing bedrock (carbonate) scarps preserved through the Holocene (*Roberts and Michetti*, 2004). Bedrock fault scarps are well exposed throughout this region, yet it is debated in the literature whether they should be considered active and forming due to coseismic slip (*Blumetti et al.*, 1993; *Michetti et al.*, 2000; *Schlagenhauf et al.*, 2010; *Vittori et al.*, 2011) or inactive and forming through geomorphic processes such as landslides (*Anzidei et al.*, 1999; *Cinti et al.*, 1999; *Chiaraluce et al.*, 2003). For example, the Database of Individual Seismogenic Sources (DISS; *Basili et al.*, 2008) does not use the surface traces of faults offsetting bedrock geology and/or Holocene slopes to delineate the locations and geometries of active faults. Instead fault traces are simplified into rectangles or boxes that encompass the locations of fault slip from historical earthquakes or those defined by palaeoseismology (see Figure 1). In contrast, other fault databases define fault locations and geometries using observations of offset bedrock geology and Holocene slopes (e.g. *Piccardi et al.*, 1999; *Galadini and Galli*, 2000; *Vittori et al.*, 2000; *Boncio et al.*, 2004; *Roberts and Michetti*, 2004; *Faure Walker et al.*, 2010). In this paper, we investigate a well-exposed bedrock scarp in Umbria associated

65 with an earthquake in 1997 that shows evidence of surface ruptures to help resolve this
66 controversy.
67
68 From September 1997 until April 1998 there was a prolonged seismic sequence in the
69 Umbria region, centred on the town of Colfiorito (the mainshocks are shown in Figure
70 1). Earthquakes occurred over a north-west to south-east elongated zone approximately
71 40km long (*Amato et al.*, 1998; *Deschamps et al.*, 2000; *Ripepe et al.*, 2000). There were
72 three mainshocks during the sequence with M_w>5.5; Event 1 at 00:33 on the 26th
73 September 1997 (M_w=5.7), Event 2 at 09:40 on the 26th September 1997 (M_w=6.0) and
74 Event 3 at 15:23 on the 14th October (M_w=5.6). Surface effects of the three mainshocks
75 were widely recorded in the epicentral region immediately after the earthquakes
76 occurred (*Basili et al.*, 1998; *Cello et al.*, 1998; *Vittori et al.*, 2000). Such effects included
77 cracking of road and the ground surface, open fissures, alluvial scarps, landslides, and
78 the appearance of a brown, soil-covered, stripe at the base of the bedrock scarp. This
79 stripe is now visible as a pale unweathered stripe at the base of the MLS fault (Figure 1
80 and 2). A similar pale stripe can be observed along the north-west section of the CSM
81 fault (Figure 1). There is some controversy regarding joining the surface observations
82 to the first two main shocks. *Chiaraluce et al.* (2005) hypothesise that Event 1 occurred
83 on the MLS fault. However according to the observations of the CSM fault before and
84 after Event 2 (*Cello et al.*, 1998) the surface effects were the same, hence they associate
85 Event 1 with the CSM fault. However when the earthquake hypocentre are plotted in
86 relation to the surface expressions of the faults, Event 1 occurred almost directly
87 beneath the CSM fault (Figure 1). This does not support Event 1 located on the CSM
88 fault. One possibility is that Event 1 was a composite rupture of the MLS and CSM faults.
89 Event 2 is also likely to be located on the MLS based on the hypocentre locations. Some

90 authors argue that the stripe at the base of the fault scarp results from coseismic slip
91 from a mainshock event (*Cello et al.*, 1998, 2000; *Vittori et al.*, 2000). In contrast, other
92 authors argue that all surface effects are secondary (i.e. non-tectonic). *Cinti et al.*, 2000
93 argue for broad NW-SE zones of deformation, comprising of surface breaks and
94 landslides, these zones partially coincide with the active fault traces in Figure 1. *Basili et*
95 *al.* (1998) argue that the stripe described formed due to compaction of debris and lower
96 slope deposits, because their observations suggested that the direction of movement
97 was parallel to the maximum slope direction.
98
99 This paper tests whether the fresh stripe is produced by compaction or primary
100 tectonic slip using theory that describes the geometry and kinematics of faulting and
101 how this controls magnitudes of surface slip (*Faure Walker et al.*, 2009). Active faults in
102 the Italian Apennines and central Greece show variability in their structure on a range
103 of scales, including metre to kilometre scale corrugations and variations in the Holocene
104 throw and slip direction along faults (*Roberts and Michetti*, 2004; *Roberts*, 2007; *Faure*
105 *Walker et al.*, 2009; *Wilkinson et al.*, 2015). Faure Walker *et al.* (2009) demonstrated a
106 quantitative relationship showing that strike, dip, Holocene throw and the slip vector of
107 a fault are interrelated. Assuming that the principal strain rate is constant across a fault,
108 if the strike becomes more oblique to the regional principal strain, for example around a
109 bend in the fault plane, the throw rate of the fault will vary in order to preserve the
110 principal strain rate (*Faure Walker et al.*, 2009). This theory is summarised in Figure 2
111 as a block diagram of a simple fault, more detail can be found in Faure Walker *et al.*
112 (2009). This highlights the importance for knowing the local fault geometry if the total
113 throw of a fault is used as a proxy for the activity of a fault. This relationship has the
114 potential to differentiate between compaction and tectonic slip as the cause of the fresh

stripe of rock along the bottom of the fault scarp. For the former, slip will show no relationship with the geometry and kinematics of bedrock faulting but may correlate with the hillside geomorphology, whilst for the latter we expect coseismic throw to increase where the strike and dip of the fault plane change relative to the slip-vector but should not show a correlation with the hillslope.

To study the above, high-spatial-resolution structural data has been collected, supported by TLS (Terrestrial Laser Scanning) of the geomorphology and slopes, along the Mt Le Scalette fault, situated on the Umbria-Marche regional border, near the town of Colfiorito. This fault (Figure 1) ruptured during at least one of the mainshocks of 1997 (Event 1 and/or Event 2), and is suggested by some to have ruptured at the surface (*Cello et al.,* 1998; *Vittori et al.,* 2000). We first review the structural setting of the earthquake before proceeding to an analysis of structural measurements on the bedrock faults and discussion of their link to the nodal plane dips for the earthquakes.

2. Geological background

The Italian Apennines are undergoing continental extension, located between the converging African and Eurasian plates (*Anderson and Jackson*, 1987). There is a narrow zone of convergence and thrusting along the Adriatic coast at the present day, whereas inland the thrusting ceased during the Pliocene (*Patacca et al.*, 1990). Present day extension began 2.5 Ma, evident by sediment and fossils infilling extensional basins (*Cavinato et al.*, 2002; *Roberts and Michetti*, 2004), defined by a series of normal faults striking north-west to south-east. The Italian peninsula has undergone long wavelength uplift since the early Pleistocene (*Girotti and Piccardi*, 1994; *Coltorti and Pieruccini*, 2000; *D'Agostino et al.*, 2001), and the distribution and strain-rates associated with the

140 active faults correlates with this long wavelength topography (*Faure Walker et al.*, 2012;
141 *Cowie et al.*, 2013).
142
143 Bedrock scarps in Mesozoic limestone are well-exposed in the Italian Apennines. It is
144 hypothesised that these scarps are formed by tectonic exhumation and preserved since
145 the end of the Last Glacial Maximum (LGM, 15±3 kyr) due to decreasing erosion rates
146 (*Piccardi et al.*, 1999; *Galadini and Galli*, 2000; *Roberts and Michetti*, 2004, fig.7; *Tucker*
147 *et al.*, 2011). This is confirmed by in situ ^{36}Cl cosmogenic isotope studies of the
148 exhumation of the fault planes (*Palumbo et al.*, 2004, *Schlagenhauf et al.*, 2010, 2011).
149
150 In Umbria, the Mt Le Scalette and the Costa-San Martino faults form bedrock scarps in
151 Jurassic and Cretaceous limestones, with Oligocene sediments exposed in the hanging
152 walls. The stratigraphic throws across the Mt Le Scalette and Costa-San Martino faults
153 are 550-600m (*Mirabella et al.*, 2005). The Mt Le Scalette fault borders the internally
154 draining Colfiorito basin (*Calamita et al.*, 2000; *D'Agostino et al.*, 2009). The last known
155 earthquake prior to 1997 in the area surrounding these faults was in 1279 A.D. (*Boschi*,
156 2000; *Guidoboni et al.*, 2007), but it is not possible to assign this earthquake
157 conclusively to either fault due to sparse shaking records (*Guidoboni et al.*, 2007) and a
158 lack of paleoseismic trenching on either fault. Instrumentally recorded earthquakes
159 (1979 Norcia fault M_w=5.8; 1984 Gubbio fault M_w=5.6; 1997 Colfiorito earthquakes,
160 $M_w \leq 6.0$; *Deschamps et al.*, 1984; *Westaway et al.*, 1989) all show normal faulting
161 mechanisms, which is consistent with the present day tectonic extension (*Anderson and*
162 *Jackson*, 1987; *Boncio et al.*, 2004; *D'Agostino et al.*, 2009). Here we concentrate on un-
163 weathered stripes of exposed bedrock that are known to have been exhumed during the

earthquake sequence, in an attempt to ascertain whether they have been exhumed by compaction or primary tectonic slip that can be linked to an earthquake at depth.

3. Methods

Detailed structural mapping was undertaken on the Mt Le Scalette fault (Figure 1) using a handheld Garmin GPS to record UTM coordinates of localities along the fault scarp, with a location accuracy of approximately ±5m. Structural data were measured on all exposed fault surfaces. Strike, dip and kinematic measurements were taken using a compass-clinometer along the fault scarp; these measurements have an accuracy of ±2°. Slip-vector azimuth measurements were taken from frictional wear striae on the bedrock scarps and from the geometry of large and small-scale corrugations. Previously Roberts (2007) has shown that where striae and corrugations are measured at the same locations on other faults in Italy and Greece, the same azimuth is recovered from each feature. Note that the fault slip-vector studied must be measured on the bedrock scarp itself and clearly be part of the structural geology of the fault. Thus, we measure the slip vector from frictional wear striae and corrugations associated with slickenslides on the bedrock. In contrast, Basili *et al.* (1998) measure displacements arising from soil sliding along planes coincident with the fault plane and they observe that the direction of displacements always seem to be parallel to the direction of maximum slope. We are aware that slip-vectors measured from deformed soils can converge into incised hangingwall gullies, suggesting overall down-slope movements (*Basili et al.*, 1998), but we specifically do not measure from such locations as they do not un-ambiguously record the tectonic slip vector, but rather record gravitationally-induced shallow mass wasting. At the base of the Mt Le Scalette scarp, a pale unweathered stripe is observed (Figure 3). The slip associated with this stripe was measured using a ruler. The upper

edge of the stripe is defined where weathering increases over a few millimetres to centimetres to its top edge and the first occurrence of moss. The base is defined by the transition to soil in the hangingwall. We define the error in these measurements to be ±2 cm (see Fig. 2e and f for detail). The height of the stripe in the plane of the scarp (slip) was measured in the field and converted to vertical height (throw; using the measured dip). The structural data were analysed using Stereonet 8 (*Allmendinger et al.*, 2012). A structural map was constructed in the field, noting the location and extent of fans, gullies and other geomorphic features. Structural data from the bedrock scarp were added to this map following post-field analysis.

3.1. Terrestrial Laser Scanning

TLS data enabled us to interpret the surface geomorphology on a portion of the fault. The fault surface, footwall and hangingwall topography was captured as x-y-z coordinate point clouds using a Leica Scanstation C10 instrument. In addition to background intensity values, an onboard digital camera automatically acquired colour images that were used to RGB colour-code the point cloud data. Six separate scans were acquired in three different locations containing c. 30 million individual points in total. Scans were co-registered to a network of reflectors placed within the point cloud. The location of each reflector was surveyed using a differential GNSS and during post processing converted into the Universal Transverse Mercator (UTM) coordinate system (Zone 33 T). Individual scans were combined in Leica Geosystems HDS Cyclone™ software. To remove vegetation, the point cloud data was processed using a box-filter with three different box sizes depending on the density of point within the grid-area sampled. For areas of the point cloud where the number of points per m^2 was less than 2000, the lowest point in a 4 m^2 area was selected. Where the point cloud density was

214 less than 10,000 points per m^2, the lowest point in every $1m^2$ was selected. For a greater
215 density, the lowest point in every 0.5 m^2 was selected. Manual filtering was then used to
216 remove any remnants of vegetation from the point cloud. A digital elevation model
217 (DEM) was created by converting the filtered point cloud to a triangulated irregular
218 network (TIN) and then to raster format by gridding the data at 1m resolution within a
219 geographical information system (GIS). Two $10m^2$ areas were selected on the
220 hangingwall and footwall slopes and aspect analysis were performed within the GIS. A
221 topographic profile was extracted and interpreted from the raw TLS point cloud data.
222
223 **4. Results**
224 4.1 Structural Mapping
225 The structural map constructed (Figure 4) shows the fault scarp trace for a 600 m long
226 section of the fault, with structural, kinematic and geomorphological data along the
227 section. The constructed map shows that there is variability in the strike of the fault
228 scarp and that corrugations/bends can be seen at many different scales. For example, a
229 large-scale corrugation that is convex to the SW exists over a distance of ~350 m along
230 strike between points B' and B on Figure 4 and is also evident on the strike versus
231 distance graph in Figure 5a. Note this variability in the trace of the fault is a real
232 corrugation (i.e. not just a change in map trace due to topography), confirmed by
233 topographic contours (Figure 4) and the field measurements taken along the fault scarp
234 (Figure 5a).
235
236 To test whether the slip-vector changes across the corrugation, the slip vector was
237 measured at four locations across the corrugation between B' and B from frictional
238 wear striae on the fault plane. The mean slip vector plunge and azimuth is 61^o towards

239 211°, with little variation between the 4 sites (< 13° variation defined by 202°, 206°,
240 212° and 215° for the azimuth values), despite the fact the strike changes by ~40°
241 across the same corrugation. Thus, it appears that the mean slip-vector is in accord with
242 the resolved shear strain from the larger-scale strain tensors on the fault plane (e.g.
243 *Roberts*, 1996a, 1996b, 2007) and is unaffected by small-scale variations in fault
244 geometry.
245
246 In order to test whether the slip-vector is related to the larger-scale strain tensors or
247 local surface slopes as suggested by Basili *et al.* (1998), we have also measured the
248 aspect (downslope direction) of the slopes around the fault scarp (Figure 4b and c). Our
249 TLS results show that the downslope direction for the lower slope shows a strong peak
250 at ~260°, whereas measurements of striae show that the mean slip-vector azimuth is
251 211° (Figure 4c). Thus, it is clear that the slip vector azimuth defined by faulting in the
252 bedrock is not perpendicular to the slope defined by the TLS data and hence
253 inconsistent with local gravity-driven compaction as the cause of the slip.
254
255 *4.2 Interpretation of structural measurements*
256 From the data presented in Figure 5, a systematic relationship between the strike, dip
257 and coseismic throw is seen across the large-scale corrugation between B' and B
258 (Figures 5a and b). When the strike is perpendicular to the sip vector azimuth (around
259 150m along the section in Figure 5), the dip and coseismic throw are at a minimum of
260 55-65° and 3-6cm respectively. Close to the lateral extremities of the corrugation (at 0-
261 50m and 250-400m along the section in Figure 5), strikes are oblique to the tectonic slip
262 vector azimuth of 211° and the measured dips are 60-80° and coseismic throw values
263 are 7-12cm. Figure 5d confirms that the strike and dip are varying in tandem because a

positive correlation is found across this corrugation. Again this suggests that the small-scale fault geometry and slip interact in response to the larger-scale strain tensors. These results and the systematic relationship observed in Figure 5 agrees with the theory presented in Faure Walker *et al.* (2009) and shown in Figure 2 in this paper.

Thus, we have a physical explanation for the structural variation we have measured that is rooted in an established theoretical framework. This is consistent with the hypothesis that surface slip evidenced by the fresh stripe is associated with tectonic slip on the bedrock scarp and inconsistent with the hypothesis of gravity-driven slip associated with compaction. The height of the stripe at the base of the Mt Le Scalette fault is assumed to be solely due to coseismic slip, as the free faces were observed for months following the mainshocks and no additional (post-seismic) slip was detected (*Vittori et al.*, 2000).

Our interpretation of tectonic slip across the scarp, rather than slip driven by compaction, suggests that we are able to extract a value for the cumulative tectonic slip and hence the tectonic slip-rate across the fault averaged within a time period given regional constraints on the age of the offset slopes. Using an age of 15 ±3 ka for the offset paleosurface and a value of 10.11 m for the offset derived from a scarp profile from our TLS dataset (see Figure 4a), we derive a throw-rate of 0.67 ± 0.13 $mmyr^{-1}$ since the demise of the LGM.

Similar bedrock scarps have been shown to be exhumed in the Holocene in central Italy using ^{36}Cl in situ cosmogenic exposure dating (e.g. *Palumbo et al.*, 2004; *Schlagenhauf et al.*, 2010, 2011; *Benedetti et al.*, 2013). This is consistent with tephrachronology and

289 dated climate driven erosion rate changes that suggest the paleosurfaces date from the
290 time of the demise of the last glacial maximum at 15 ±3 ka (see Roberts and Michetti
291 (2004) for a review).
292
293 *4.3. Reassessment of nodal plane dips*
294
295 Cinti *et al.* (1999) suggested that the CMT dip projected from the hypocentre to the
296 surface does not align with the observed fault scarps at surface (see *Cinti et al.*, 1999,
297 fig.4). Also, Chiaraluce *et al.* (2005) proposed that there is a difference between the dips
298 measured at the surface and at depth. These two observations have been used to
299 suggest that the surface faults were not reactivated by primary tectonic slip during the
300 earthquakes. However, as shown above in Section 4.1, up to ~25° variation in fault dip
301 has been measured on the bedrock fault scarp and uncertainties exist for the
302 hypocentral locations and nodal plane dips from the seismological data. Hence the
303 ranges of surface and seismological dip data may overlap. Below we investigate
304 whether we can reconcile the seismological data from depth with those measured at the
305 surface to see if it is possible to exclude slip at depth propagating to the bedrock fault
306 scarps at the surface.
307
308 Published hypocentres and dips for the three mainshocks of 1997 are shown in Figures
309 6 and 7. There is a large range in the depth and location for the same earthquake, as
310 reported by different authors (*Amato et al.*, 1998; *Cello et al.*, 1998; *Boncio and*
311 *Lavecchia*, 2000b; *Cattaneo et al.*, 2000; *Cocco et al.*, 2000; *Castello et al.*, 2006;
312 *Chiarabba et al.*, 2009); this is due to different location methods, velocity models and
313 station arrays being used. One set of hypocentres presented are preliminary locations

(*Cello et al.*, 1998) and hence are less reliable than later location studies. Another set of hypocentres are based on worldwide teleseismic arrivals (*ISC*, 2012) and are likely to have poorer location constraints. Certain locations are more precise than others, due to the use of a double difference location method (*Waldhauser and Ellsworth*, 2000) as used by *Chiaraluce et al.* (2003) and *Chiarabba et al.* (2009), or due to using a local network (*Cattaneo et al.*, 2000), or a 3D velocity model (*Chiarabba et al.*, 2009). Furthermore, for nodal plane dips, studies have concentrated on results computed by different moment tensor inversions (e.g. *Ekström et al.*, 1998; *Weston et al.*, 2011), fitting focal planes to arrival polarities (*Cattaneo et al.*, 2000), and from the aftershocks (*Chiaraluce et al.*, 2005). The range of dip values published in the literature is up to 23^{o} for a single event. Dip values obtained from aftershock alignment are reported in Chiaraluce *et al.* (2005). The aftershocks form a diffuse but planar alignment in the upper 7-8km of the crust. (see fig. 7, in *Chiaraluce et al.*, 2005). Hence the range in dips from aftershock alignment can be up to 30^{o}.

Some authors have suggested that the normal faults in the Apennines have a listric dip (*Boncio and Lavecchia*, 2000b; *Barchi and Mirabella*, 2009) based on seismic reflection profiles from Bally *et al.* (1986). This could reconcile the difference in dips between the surface measurements and nodal plane dips. However, studies of aftershock locations from the L'Aquila (*Valoroso et al.*, 2013), Colfiorito (*Chiaraluce et al.*, 2003) and Gualdo Tadino (*Ciaccio et al.*, 2005) earthquake sequences show that the aftershock alignments favour a planar fault at depth.

Taken together, we have compared hypocentral locations and nodal plane dips with measurements at the surface reported in Section 4.1. The results show that several of

339 the hypocentral locations fall within the range of the down-dip projection of the surface
340 trace of the fault from our structural measurements (i.e. within the black dashed lines
341 delineating the range of data in Figure 6) and postulated dips overlap within error
342 (Figure 7). Thus, the possibility that the earthquakes occurred on the down-dip
343 projections of the surface faults cannot be excluded. We therefore reject the hypothesis
344 that the earthquakes did not occur on the down-dip prolongation of the surface faults,
345 and support the hypothesis that the surface faults were reactivated by primary tectonic
346 slip during the earthquakes.
347
348 **5. Discussion**
349 A key question in seismic hazard is whether slip at depth in an earthquake propagates
350 to the surface. If it does, the surface trace of the fault defines the exact location and
351 geometry of a seismic source and hence can be used as an input for seismic hazard
352 assessment (e.g. *Stirling et al.*, 2002; *Cheng et al.*, 2007; *Field et al.*, 2009, for other
353 tectonically active regions). This informs modelling of slip distributions on the fault
354 surface at depth for Italian and worldwide examples (e.g. *Stramondo et al.*, 1999 for the
355 1997 Colfiorito earthquake, Wald and Heton (1994) for the 1992 Landers earthquake,
356 Ozawa *et al.* (2011) for the 2011 Tohoku earthquake) and hence expected ground
357 shaking during an earthquake (e.g. *Barba and Basili*, 2000). Until now uncertainty has
358 surrounded the question in the case of the 1997 Colfiorito earthquakes. Figure 1 shows
359 both the "individual seismogenic sources" from DISS 3.2.0 (see Basili *et al.* (2008) for
360 description of this database), and the surface traces of mapped faults that offset the
361 surface geology from Mirabella *et al.* (2005). Clearly the simplified traces from DISS will
362 yield simplified slip distributions and models of ground shaking if used in modelling
363 seismological and geodetic data if the actual trace is that of Mirabella *et al.* (2005). Our

findings herein suggest that the surface trace from Mirabella *et al.* (2005) does indeed mark the location where slip at depth propagated to the surface. We suggest that an improved understanding of the slip distribution and ground shaking would be achieved if the detailed surface fault trace were included in calculations.

Our results are not surprising. Surface faulting has been widely reported for a number of normal faulting earthquakes in the USA (e.g. DePolo *et al.* (1991) for a summary and Wallace *et al.* (1984) for the 1915 Pleasant Valley earthquake), Greece (e.g. *Jackson et al.*, 1982), Turkey (e.g. *Eyidogan and Jackson*, 1985),and Italy (1915 Fucino (*Oddone*, 1915; *Galadini et al.*, 1997) and 2009 L'Aquila (*Wilkinson et al.*, 2010; *Vittori et al.*, 2011)). It is widely believed that these are the primary surface expression of slip at depth propagating to the surface (*Jackson and White*, 1989; *Wells and Coppersmith*, 1994). Despite this, some examples from Italy of hypothesised primary surface slip have been rejected by some, usually with reference to the possible effects of ground-shaking and compaction producing surface rupture (e.g. Basili et al. (1998) and Barba and Basili (2000) for the 1997 Colfiorito earthquakes) or that the faults are sealed by Quaternary deposits (e.g. *Fubelli et al.*, 2009). If this were correct, it would suggest that there is something fundamentally different about normal faulting in Italy and this would be very significant if proven by observations. However, the findings of this paper suggest that for one of the best constrained examples from Italy, faulting at depth did indeed propagate to the surface, resembling the cases from tectonic settings listed above, and suggesting there is nothing fundamentally different about normal faulting in Italy.

The quantitative relationship presented in Faure Walker *et al.* (2009) demonstrates how the strike, dip and throw are interrelated along a fault trace while maintaining a

389 constant principal strain rate. Specifically, the geometry-dependent throw-rate theory
390 hypothesises that the average Holocene throw-rate increases across the fault where the
391 deviation of the fault strike from the mean direction and the dip of the fault increases if
392 the slip vector remains constant (*Faure Walker et al., 2009, 2015*). This relationship has
393 been demonstrated for two faults in the central Apennines that display significant strike
394 variations: the Parasano Fault (*Faure Walker et al., 2009*) and the Campo Felice Fault
395 (*Wilkinson et al., 2015*). Faure Walker *et al.* (2009) noted the importance of strain rates
396 controlling seismic hazard for a particular fault and hence care must be taken if the total
397 throw is used as a proxy for the level of fault activity because of local geometry. The
398 data presented in this paper is the first known example of a coseismic slip distribution
399 broadly agreeing with the relationship and hence improves the reliability of the
400 relationship.
401
402 We make three points that have wider significance:
403
404 1) This work highlights the difficulty of resolving subjective interpretations of surface
405 deformation that do not involve structural geological analysis. We outline an approach
406 where the question of primary surface faulting resulting from propagation of slip from
407 depth can be assessed within a quantitative structural geology framework derived from
408 theory that describes the geometric aspects of slip on non-planar, segmented faults in
409 relation to strain tensors (*Faure Walker et al.*, 2009). We suggest that, where possible,
410 (a) in the future, measurements of the strike, dip and slip-vector of bedrock faults
411 associated with surface ruptures should be routinely measured before assessing surface
412 ruptures as the result of primary surface faulting or ruptures resulting from shaking

413 and compaction, and (b) that other examples in the literature, especially in Italy (e.g.
414 Basili *et al.* (1998) and Barba and Basili (2000)) should be revisited with this in mind.
415
416 2) We note that many examples exist in the literature (see Galli *et al.* (2008) for a
417 review) where values for coseismic throw have been derived by palaeoseismologists for
418 ancient earthquakes in the absence of discussion of the fault geometry and kinematics.
419 This approach used herein suggests that values for coseismic throw measured from
420 palaeoseismology need to be re-assessed taking into account whether the throw value
421 comes from a location where the local fault geometry has produced anomalously large
422 slip such as where the slip vector is not perpendicular to the fault trace, or a location
423 that is more typical of the earthquake in question (see also *Faure Walker et al.*, 2015).
424
425 3) It is only possible to use observations of offset geomorphology of known age to infer
426 rates of tectonic deformation if the surface offsets are produced by primary surface slip
427 rather than gravity-driven compaction. Our observations suggest primary slip
428 propagates to the surface, consistent with observations of ^{36}Cl in situ cosmogenic
429 exposure dating on similar fault scarps in Italy (*Palumbo et al.*, 2004; *Schlagenhauf et al.*,
430 2010, 2011; *Benedetti et al.*, 2013). Suggestions to the contrary where surface
431 deformation is hypothesised to result from gravity driven compaction during shaking
432 invalidate the approach of tectonic geomorphology if correct; thus, such interpretations
433 must be made with extreme caution. In this example we report that we reject the
434 hypothesis that surface deformation is produced instead by gravity driven compaction
435 during shaking. This allows us to derive a throw-rate averaged over many seismic cycles
436 (15 ±3 ka) that would otherwise be dismissed. Our findings suggest that the approach

taken by tectonic geomorphologists is valid for this example, and also for other areas affected by normal faulting in Italy.

Overall, we suggest that with careful field structural geology, it is possible to gain insights into the normal faulting earthquakes that would be unavailable without the detailed structural mapping presented herein.

6. Conclusions

In this paper we present structural data from a surface bedrock scarp that displays a systematic relationship between the fault geometry and the coseismic throw. Hence we conclude that this fault scarp, and others that are exposed in the Apennines, are active and connected to the seismogenic structure at depth, agreeing with previously published work (e.g. Blumetti *et al.* (1993); Michetti *et al.* (2000); Vittori *et al.* (2011)). This is an important debate to resolve, as it has implications for utilising active fault traces for seismic hazard assessment in the region. This conclusion is not surprising when compared with other active normal fault systems around the world, such as the Basin and Range, Greece and Turkey. Our structural measurements from the Mt Le Scalette fault scarp highlight that the fault geometry and (coseismic) throw is systematically variable from metre to hundreds of metres scale. This is rarely appreciated or considered in other examples of faults in the Apennines, particularly in the field of paleoseismology. Coseismic slip is measured in paleoseismic trenches and can be used to infer the magnitude of past events (e.g. Galli *et al.* (2008)). However, without knowledge of the fault geometry at the trench location, the magnitude may be incorrectly estimated. Our conclusion also agrees with ^{36}Cl cosmogenic dating performed on similar bedrock scarps in Italy for two reasons. Firstly the exposure ages

462 calculated from ^{36}Cl concentration indicate exposure throughout the Holocene, hence
463 the faults are not inactive in the Holocene or sealed as suggested by some authors
464 (*Fubelli et al.*, 2009). Secondly the exposure results obtained can only be explained by a
465 coseismic slip history and not by a landslide or compaction history. Hence for any
466 investigation of the active tectonics and paleo-earthquakes in the Italian Apennines we
467 conclude that it is important to understand and analyse the local fault geometry so that
468 results are valid.
469
470 **Acknowledgments**
471 This study was funded by the NERC Studentship NE/L501700/1 and the NERC grants
472 (NE/E01545X/1 and NE/I024127/1). Comments from Laura Gregory (University of
473 Leeds) helped to improve the manuscript.
474
475 **References:**
476 Allmendinger, R. W., N. Cardozo, and D. M. Fisher (2012), *Structural Geology Algorithms:*
477 *Vectors and tensors*, 1st ed., Cambridge University Press.

478 Amato, A., R. Azzara, C. Chiarabba, G. B. Cimini, M. Cocco, M. Di Bona, L. Margheriti, S.
479 Mazza, F. Mele, G. Selvaggi, A. Basili, E. Boschi, F. Courboulex, A. Deschamps, S.
480 Gaffet, G. Bittarelli, L. Chiaraluce, D. Piccinini, and M. Ripepe (1998), The 1997
481 Umbria-Marche, Italy, earthquake sequence: A first look at the main shocks and
482 aftershocks, *Geophys. Res. Lett.*, *25*(15), 2861–2864.

483 Anderson, H., and J. A. Jackson (1987), Active tectonics of the Adriatic Region, *Geophys. J.*
484 *Int.*, *91*, 937–983.

485 Anzidei, M., P. Baldi, A. Galvani, A. Pesci, I. Hunstad, and E. Boschi (1999), Coseismic

displacement of the 27th September 1997 Umbria-Marche (Italy) earthquakes detected by GPS: campaigns and data, *Ann. di Geofis.*, *42*(4), 597–607.

Bally, A. W., L. Burbi, C. Cooper, and R. Ghelardoni (1986), Balanced sections and seismic reflection profiles across the Central Apennines, *Mem. Soc. Geol. It*, *35*(1), 257–310.

Barba, S., and R. Basili (2000), Analysis of seismological and geological observations for moderate-size earthquakes: The Colfiorito Fault System (Central Apennines, Italy), *Geophys. J. Int.*, *141*(1), 241–252, doi:10.1046/j.1365-246X.2000.00080.x.

Barchi, M. R., and F. Mirabella (2009), The 1997–98 Umbria–Marche earthquake sequence: "Geological" vs. "seismological" faults, *Tectonophysics*, *476*(1-2), 170–179, doi:10.1016/j.tecto.2008.09.013.

Basili, R., V. Bosi, F. Galadini, P. Galli, M. Meghraoui, P. Messina, M. Moro, and A. Sposato (1998), The Colfiorito Earthquake Sequence of September–October 1997: Surface Breaks and Seismotectonic Implications for the Central Apennines (Italy), *J. Earthq. Eng.*, *2*(January 2015), 291–302, doi:10.1080/13632469809350323.

Basili, R., G. Valensise, P. Vannoli, P. Burrato, U. Fracassi, S. Mariano, M. M. Tiberti, and E. Boschi (2008), The Database of Individual Seismogenic Sources (DISS), version 3: Summarizing 20 years of research on Italy's earthquake geology, *Tectonophysics*, *453*(1-4), 20–43, doi:10.1016/j.tecto.2007.04.014.

Benedetti, L., I. Manighetti, Y. Gaudemer, R. Finkel, J. Malavieille, K. Pou, M. Arnold, G. Aumaître, D. Bourlès, and K. Keddadouche (2013), Earthquake synchrony and clustering on Fucino faults (Central Italy) as revealed from in situ 36 Cl exposure dating, *J. Geophys. Res. Solid Earth*, *118*(9), 4948–4974, doi:10.1002/jgrb.50299.

Blumetti, A. M., F. Dramis, and A. M. Michetti (1993), Fault-generated mountain fronts in

509 the central apennines (Central Italy): Geomorphological features and
510 seismotectonic implications, *Earth Surf. Process. Landforms*, *18*(3), 203–223,
511 doi:10.1002/esp.3290180304.

512 Boncio, P., and G. Lavecchia (2000a), A geological model for the Colfiorito earthquakes
513 (September-October 1997, central Italy), *J. Seismol.*, *4*, 345–356.

514 Boncio, P., and G. Lavecchia (2000b), A structural model for active extension in Central
515 Italy, *J. Geodyn.*, *29*, 233–244.

516 Boncio, P., G. Lavecchia, and B. Pace (2004), Defining a model of 3D seismogenic sources
517 for Seismic Hazard Assessment applications: The case of central Apennines (Italy),
518 *J. Seismol.*, *8*(3), 407–425, doi:10.1023/B:JOSE.0000038449.78801.05.

519 Boschi, E. (2000), Earthquake of 30 April 1279, Umbria-Marche Apennines, *Ann. di*
520 *Geofis.*, *43*.

521 Calamita, F., M. Coltorti, D. Piccinini, P. P. Pierantoni, A. Pizzi, M. Ripepe, V. Scisciani, and
522 E. Turco (2000), Quaternary faults and seismicity in the Umbro-Marchean
523 Apennines (Central Italy): Evidence from the 1997 Colfiorito earthquake, *J. Geodyn.*,
524 *29*(3-5), 245–264, doi:10.1016/S0264-3707(99)00054-X.

525 Castello, B., G. Selvaggi, C. Chiarabba, and A. Amato (2006), CSI Catalogo della sismicità
526 italiana 1981-2002, *INGV-CNT Roma*. Available from:
527 http://csi.rm.ingv.it/versione_inglese/index_eng.htm

528 Cattaneo, M., P. Augliera, G. De Luca, A. Gorini, A. Govoni, S. Marcucci, A. Michelini, G.
529 Monachesi, D. Spallarossa, and L. Trojani (2000), The 1997 Umbria-Marche (Italy)
530 earthquake sequence: Analysis of the data recorded by the local and temporary
531 networks, *J. Seismol.*, *4*, 401–414.

532 Cavinato, G. P., C. Carusi, M. Dall'asta, E. Miccadei, and T. Piacentini (2002), Sedimentary
533 and tectonic evolution of Plio-Pleistocene alluvial and lacustrine deposits of Fucino
534 Basin (central Italy), *Sediment. Geol.*, *148*, 29–59, doi:10.1016/S0037-
535 0738(01)00209-3.

536 Cello, G., G. Deiana, P. Mangano, S. Mazzoli, E. Tondi, L. Ferreli, L. Maschio, A. M. Michetti,
537 L. Serva, and E. Vittori (1998), Evidence for surface faulting during the September
538 26, 1997, Colfiorito (central Italy) earthquakes, *J. Earthq. Eng.*, *2*(2), 303–324,
539 doi:10.1080/13632469809350324.

540 Cello, G., G. Deiana, L. Ferelli, L. Marchegiani, L. Maschio, S. Mazzoli, A. M. Michetti, L.
541 Serva, E. Tondi, and T. Vittori (2000), Geological constraints for earthquake faulting
542 studies in the Colfiorito area (central Italy), *J. Seismol.*, *4*, 357–364.

543 Cheng, C.-T., S.-J. Chiou, C.-T. Lee, and Y.-B. Tsai (2007), Study on Probabilistic Seismic
544 Hazard Maps of Taiwan after Chi Chi Earthquake, *J. Geoengin.*, *2*(1), 19–28,
545 doi:10.6310/jog.2007.2(1).3.

546 Chiarabba, C., D. Piccinini, and P. De Gori (2009), Velocity and attenuation tomography
547 of the Umbria Marche 1997 fault system: Evidence of a fluid-governed seismic
548 sequence, *Tectonophysics*, *476*(1-2), 73–84, doi:10.1016/j.tecto.2009.04.004.

549 Chiaraluce, L., W. L. Ellsworth, C. Chiarabba, and M. Cocco (2003), Imaging the
550 complexity of an active normal fault system: The 1997 Colfiorito (central Italy) case
551 study, *J. Geophys. Res.*, *108*(B6), 2294, doi:10.1029/2002JB002166.

552 Chiaraluce, L., M. R. Barchi, C. Collettini, F. Mirabella, and S. Pucci (2005), Connecting
553 seismically active normal faults with Quaternary geological structures in a complex
554 extensional environment: The Colfiorito 1997 case history (northern Apennines,

555 Italy), *Tectonics*, *24*(1), doi:10.1029/2004TC001627.

556 Ciaccio, M. G., M. R. Barchi, C. Chiarabba, F. Mirabella, and E. Stucchi (2005),
557 Seismological, geological and geophysical constraints for the Gualdo Tadino fault,
558 Umbria–Marche Apennines (central Italy), *Tectonophysics*, *406*(3-4), 233–247,
559 doi:10.1016/j.tecto.2005.05.027.

560 Cinti, F. R., L. Cucci, F. Marta, and P. Montone (1999), The 1997 Umbria-Marche (Italy)
561 earthquake sequence: relationship between ground deformation and seismogenic
562 structure., *Geophys. Res. Lett.*, *26*(7), 895–898.

563 Cinti, F. R., L. Cucci, F. Marra, and P. Montone (2000), The 1997 Umbria-Marche
564 earthquakes (Italy): Relation between the surface tectonic breaks and the area of
565 deformation, *J. Seismol.*, *4*(4), 333–343, doi:10.1023/A:1026575219394.

566 Cocco, M., C. Nostro, and G. Ekström (2000), Static stress changes and fault interaction
567 during the 1997 Umbria-Marche earthquake sequence, *J. Seismol.*, *4*, 501–516.

568 Coltorti, M., and P. Pieruccini (2000), A late Lower Pliocene planation surface across the
569 Italian Peninsula: A key tool in neotectonic studies, *J. Geodyn.*, *29*(3-5), 323–328,
570 doi:10.1016/S0264-3707(99)00049-6.

571 Cowie, P. A., C. H. Scholz, G. P. Roberts, J. P. Faure Walker, and P. Steer (2013), Viscous
572 roots of active seismogenic faults revealed by geologic slip rate variations, *Nat.*
573 *Geosci.*, *6.12*(November), 1036–1040, doi:10.1038/ngeo1991.

574 D'Agostino, N., J. A. Jackson, F. Dramis, and R. Funiciello (2001), Interactions between
575 mantle upwelling, drainage evolution and active normal faulting: an example from
576 the central Apennines (Italy), *Geophys. J. Int.*, *147*(2), 475–497, doi:10.1046/j.1365-
577 246X.2001.00539.x.

578 D'Agostino, N., S. Mantenuto, E. D'Anastasio, A. Avallone, M. R. Barchi, C. Collettini, F.
579 Radicioni, A. Stoppini, and G. Fastellini (2009), Contemporary crustal extension in
580 the Umbria–Marche Apennines from regional CGPS networks and comparison
581 between geodetic and seismic deformation, *Tectonophysics*, *476*, 3–12,
582 doi:10.1016/j.tecto.2008.09.033.

583 DePolo, C. M., D. G. Clark, D. B. Slemmons, and A. R. Ramelli (1991), Historical surface
584 faulting in the Basin and Range province, western North America: implications for
585 fault segmentation, *J. Struct. Geol.*, *13*(2), 123–136, doi:10.1016/0191-
586 8141(91)90061-M.

587 Deschamps, A., G. Iannacoone, and R. Scarpa (1984), The Umbrian earthquake (Italy) of
588 19 September 1979, *Ann. Geophys.*, *2*(1), 29–36.

589 Deschamps, A., F. Courboulex, S. Gaffet, A. Lomax, J. Virieux, A. Amato, A. Azzara, C.
590 Chiarabba, G. B. Cimini, M. Cocco, M. Di Bona, L. Margheriti, F. Mele, L. Chiaraluce, D.
591 Piccinini, and M. Ripepe (2000), Spatio-temporal distribution of seismic activity
592 during the Umbria-Marche crisis, 1997, *J. Seismol.*, 377–386.

593 Dziewonski, A. M., G. Ekström, and N. N. Maternovskaya (2003), Centroid-moment
594 tensor solutions for July–September 1997, *Phys. Earth Planet. Inter.*, *136*(3-4), 119–
595 131, doi:10.1016/S0031-9201(03)00031-1.

596 Ekström, G., A. Morelli, E. Boschi, and A. M. Dziewonski (1998), Moment tensor analysis
597 of the central Italy earthquake sequence of September-October 1997, *Geophys. Res.*
598 *Lett.*, *25*(11), 1971–1974.

599 Eyidogan, H., and J. A. Jackson (1985), A seismological study of normal faulting in the
600 Demirci, Alasehir and Gediz earthquakes of 1969-70 in western Turkey:

601 implications for the nature and geometry of deformation in the continental crust,
602 *Geophys. J. Int.*, *81*(3), 569–607, doi:10.1111/j.1365-246X.1985.tb06423.x.

603 Faure Walker, J., G. P. Roberts, and K. J. W. Mccaffrey (2015), Long-term strain rates as a
604 tool for understanding the mechanics of continental extension and the importance
605 of local 3D fault geometry for local throw-rates across faults, *INQUA Focus Gr.*
606 *Paleoseismology Act. Tectonics*.

607 Faure Walker, J. P., G. P. Roberts, P. A. Cowie, I. D. Papanikolaou, P. R. Sammonds, A. M.
608 Michetti, and R. J. Phillips (2009), Horizontal strain-rates and throw-rates across
609 breached relay zones, central Italy: Implications for the preservation of throw
610 deficits at points of normal fault linkage, *J. Struct. Geol.*, *31*(10), 1145–1160,
611 doi:10.1016/j.jsg.2009.06.011.

612 Faure Walker, J. P., G. P. Roberts, P. R. Sammonds, and P. A. Cowie (2010), Comparison of
613 earthquake strains over 10 2 and 10 4 year timescales: Insights into variability in
614 the seismic cycle in the central Apennines, Italy, *J. Geophys. Res.*, *115*(B10), B10418,
615 doi:10.1029/2009JB006462.

616 Faure Walker, J. P., G. P. Roberts, P. A. Cowie, I. D. Papanikolaou, A. M. Michetti, P. R.
617 Sammonds, M. Wilkinson, K. J. W. McCaffrey, and R. J. Phillips (2012), Relationship
618 between topography, rates of extension and mantle dynamics in the actively-
619 extending Italian Apennines, *Earth Planet. Sci. Lett.*, *325-326*, 76–84,
620 doi:10.1016/j.epsl.2012.01.028.

621 Field, E. H., T. E. Dawson, K. R. Felzer, A. D. Frankel, V. Gupta, T. H. Jordan, T. Parsons, M.
622 D. Petersen, R. S. Stein, R. J. Weldon, and C. J. Wills (2009), Uniform California
623 earthquake rupture forecast, version 2 (UCERF 2), *Bull. Seismol. Soc. Am.*, *99*(4),
624 2053–2107, doi:10.1785/0120080049.

625 Fubelli, G., S. Gori, E. Falcucci, F. Galadini, and P. Messina (2009), Geomorphic signatures
626 of recent normal fault activity versus geological evidence of inactivity: Case studies
627 from the central Apennines (Italy), *Tectonophysics*, *476*(1-2), 252–268,
628 doi:10.1016/j.tecto.2008.10.026.

629 Galadini, F., and P. Galli (2000), Active Tectonics in the Central Apennines (Italy)– Input
630 Data for Seismic Hazard Assessment, *Nat. Hazards*, *22*, 225–270.

631 Galadini, F., P. Galli, and C. Giraudi (1997), Geological investigations of Italian
632 earthquakes: new paleoseismological data from the Fucino Plain (central Italy), *J.*
633 *Geodyn.*, *24*, 87–103.

634 Galli, P., F. Galadini, and D. Pantosti (2008), Twenty years of paleoseismology in Italy,
635 *Earth-Science Rev.*, *88*(1-2), 89–117, doi:10.1016/j.earscirev.2008.01.001.

636 Girotti, O., and L. Piccardi (1994), Linee di riva del Pleistocene inferiore sul versante
637 sinistro della Media Valle del fiume Tevere, *Quat.*, *7*, 525–536.

638 Guidoboni, E., G. Ferrari, D. Mariotti, A. Comastri, G. Tarabusi, and G. Valensise (2007),
639 CFTI4Med, Catalogue of Strong Earthquakes in Italy (461B.C.-1997) and
640 Mediterranean Area (760B.C.-1500), *INGV-SGA*. Available from:
641 http://storing.ingv.it/cfti4med/

642 ISC (2012), International Seismological Centre, On-line Bulletin, *Internatl. Seis. Cent.,*
643 *Thatcham, United Kingdom*, http://www.isc.ac.uk. Available from:
644 http://www.isc.ac.uk

645 Jackson, J. A., and N. J. White (1989), Normal faulting in the upper continental crust:
646 observations from regions of active extension, *J. Struct. Geol.*, *11*(1-2), 15–36,
647 doi:10.1016/0191-8141(89)90033-3.

Jackson, J. A., J. Gagnepain, G. Houseman, G. C. P. King, P. Papadimitriou, C. Soufleris, and J. Virieux (1982), Seismicity, normal faulting, and the geomorphological development of the Gulf of Corinth (Greece): the Corinth earthquakes of February and March 1981, *Earth Planet. Sci. Lett.*, *57*(2), 377–397, doi:10.1016/0012-821X(82)90158-3.

Michetti, A. M., L. Ferreli, E. Esposito, S. Porfido, A. M. Blumetti, E. Vittori, L. Serva, and G. P. Roberts (2000), Ground effects during the 9 September 1998, Mw=5.6, Lauria earthquake and the seismic potential of the "aseismic" Pollino region in Southern Italy, *Seismol. Res. Lett.*, *71*(1).

Mirabella, F., V. Boccali, and M. R. Barchi (2005), Segmentation and interaction of normal faults within the Colfiorito fault system (central Italy), *Geol. Soc. London, Spec. Publ.*, *243*(1), 25–36, doi:10.1144/GSL.SP.2005.243.01.04.

Oddone, E. (1915), Gli elementi fisici del grande terremoto marsicano-fucense del 13 gennaio 1915, *Boll. della Soc. Sismol. Ital.*, *19*, 71–291.

Ozawa, S., T. Nishimura, H. Suito, T. Kobayashi, M. Tobita, and T. Imakiire (2011), Coseismic and postseismic slip of the 2011 magnitude-9 Tohoku-Oki earthquake., *Nature*, *475*(7356), 373–376, doi:10.1038/nature10227.

Palumbo, L., L. Benedetti, D. Bourlès, A. Cinque, and R. Finkel (2004), Slip history of the Magnola fault (Apennines, Central Italy) from 36Cl surface exposure dating: evidence for strong earthquakes over the Holocene, *Earth Planet. Sci. Lett.*, *225*(1-2), 163–176, doi:10.1016/j.epsl.2004.06.012.

Patacca, E., R. Sartori, and P. Scandone (1990), Tyrrhenian basin and Apenninc arcs: kinematic relations since Late Tortonian times., *Mem. Soc. Geol. It*, *45*, 425–451.

671 Piccardi, L., Y. Gaudemer, P. Tapponnier, and M. Boccaletti (1999), Active oblique
672 extension in the central Apennines (Italy): evidence from the Fucino region,
673 *Geophys. J. Int.*, *139*(2), 499–530, doi:10.1046/j.1365-246x.1999.00955.x.

674 Ripepe, M., D. Piccinini, and L. Chiaraluce (2000), Foreshock sequence of The September
675 26th , 1997 Umbria-Marche earthquakes, *J. Seismol.*, 387–399.

676 Roberts, G. P. (1996a), Noncharacteristic normal faulting surface ruptures from the Gulf
677 of Corinth, Greece, *J. Geophys. Res.*, *101*, 25255–25267.

678 Roberts, G. P. (1996b), Variation in fault-slip directions along active and segmented
679 normal fault systems, *J. Struct. Geol.*, *18*(6), 835–845, doi:10.1016/S0191-
680 8141(96)80016-2.

681 Roberts, G. P. (2007), Fault orientation variations along the strike of active normal fault
682 systems in Italy and Greece: Implications for predicting the orientations of
683 subseismic-resolution faults in hydrocarbon reservoirs, *Am. Assoc. Pet. Geol. Bull.*,
684 *91*(1), 1–20, doi:10.1306/08300605146.

685 Roberts, G. P., and A. M. Michetti (2004), Spatial and temporal variations in growth rates
686 along active normal fault systems: an example from The Lazio–Abruzzo Apennines,
687 central Italy, *J. Struct. Geol.*, *26*(2), 339–376, doi:10.1016/S0191-8141(03)00103-2.

688 Roberts, G. P., P. A. Cowie, I. D. Papanikolaou, and A. M. Michetti (2004), Fault scaling
689 relationships, deformation rates and seismic hazards: an example from the Lazio–
690 Abruzzo Apennines, central Italy, *J. Struct. Geol.*, *26*(2), 377–398,
691 doi:10.1016/S0191-8141(03)00104-4.

692 Schlagenhauf, A., Y. Gaudemer, L. Benedetti, I. Manighetti, L. Palumbo, I.
693 Schimmelpfennig, R. Finkel, and K. Pou (2010), Using in situ Chlorine-36

694 cosmonuclide to recover past earthquake histories on limestone normal fault
695 scarps: A reappraisal of methodology and interpretations, *Geophys. J. Int.*, *182*(1),
696 36–72, doi:10.1111/j.1365-246X.2010.04622.x.

697 Schlagenhauf, A., I. Manighetti, L. Benedetti, Y. Gaudemer, R. Finkel, J. Malavieille, and K.
698 Pou (2011), Earthquake supercycles in Central Italy, inferred from 36Cl exposure
699 dating, *Earth Planet. Sci. Lett.*, *307*(3-4), 487–500, doi:10.1016/j.epsl.2011.05.022.

700 Stirling, M. W., G. H. McVerry, and K. R. Berryman (2002), A new seismic hazard model
701 for New Zealand, *Bull. Seismol. Soc. Am.*, *92*(5), 1878–1903,
702 doi:10.1785/0120010156.

703 Stramondo, S., M. Tesauro, P. Briole, E. Sansosti, S. Salvi, R. Lanari, M. Anzidei, P. Baldi, G.
704 Fornaro, A. Avallone, M. F. Buongiorno, G. Franceschetti, and E. Boschi (1999), The
705 September 26 , 1997 Colfiorito , Italy , earthquakes: modeled coseismic surface
706 displacement from SAR interferometry and GPS, *Geophys. Res. Lett.*, *26*(7), 883–886.

707 Tucker, G. E., S. W. McCoy, A. C. Whittaker, G. P. Roberts, S. T. Lancaster, and R. J. Phillips
708 (2011), Geomorphic significance of postglacial bedrock scarps on normal-fault
709 footwalls, *J. Geophys. Res. Earth Surf.*, *116*(F1), n/a–n/a,
710 doi:10.1029/2010JF001861.

711 Valoroso, L., L. Chiaraluce, D. Piccinini, R. Di Stefano, D. Schaff, and F. Waldhauser
712 (2013), Radiography of a normal fault system by 64,000 high-precision earthquake
713 locations: The 2009 L'Aquila (central Italy) case study, *J. Geophys. Res. Solid Earth*,
714 *118*(3), 1156–1176, doi:10.1002/jgrb.50130.

715 Vittori, E., G. Deiana, E. Esposito, L. Ferreli, L. Marchegiani, G. Mastrolorenzo, A. M.
716 Michetti, S. Porfido, L. Serva, A. L. Simonelli, and E. Tondi (2000), Ground effects

717 and surface faulting in the September-October 1997 Umbria-Marche (central Italy)
718 seismic sequence, *J. Geodyn.*, *29*, 535–564.

719 Vittori, E., P. Di Manna, A. M. Blumetti, V. Comerci, L. Guerrieri, E. Esposito, A. M.
720 Michetti, S. Porfido, L. Piccardi, G. P. Roberts, A. Berlusconi, F. Livio, G. Sileo, M.
721 Wilkinson, K. J. W. McCaffrey, R. J. Phillips, and P. A. Cowie (2011), Surface Faulting
722 of the 6 April 2009 Mw 6.3 L'Aquila Earthquake in Central Italy, *Bull. Seismol. Soc.*
723 *Am.*, *101*(4), 1507–1530, doi:10.1785/0120100140.

724 Wald, D. J., and T. H. Heton (1994), Spatial and temporal distribution of slip for the 1992
725 Landers, California, earthquake, *Bull. Seismol. Soc. Am.*, *84*(3), 668–691.

726 Waldhauser, F., and W. L. Ellsworth (2000), A Double-Difference earthquake location
727 algorithm: Method and application to the Northern Hayward Fault, California, *Bull.*
728 *Seismol. Soc. Am.*, *90*(December), 1353–1368.

729 Wallace, R. E., M. G. Bonilla, and H. A. Villalobos (1984), Faulting Related to the 1915
730 Earthquakes in Pleasant Valley, Nevada, *USGSPO*, *1274-A*.

731 Wells, D. L., and K. J. Coppersmith (1994), New Empirical Relationships among
732 Magnitude, Rupture Length, Rupture Width, Rupture Area, and Surface
733 Displacement, *Bull. Seismol. Soc. Am.*, *84*(4), 974–1002.

734 Westaway, R., R. L. Gawthorpe, and M. Tozzi (1989), Seismological and field
735 observations of the 1984 Lazio-Abruzzo earthquakes: implications for the active
736 tectonics of Italy, *Geophys. J. Int.*, *98*(3), 489–514, doi:10.1111/j.1365-
737 246X.1989.tb02285.x.

738 Weston, J., A. M. G. Ferreira, and G. J. Funning (2011), Global compilation of
739 interferometric synthetic aperture radar earthquake source models: 1.

740 Comparisons with seismic catalogs, *J. Geophys. Res.*, *116*(B8), B08408,
741 doi:10.1029/2010JB008131.

742 Wilkinson, M., K. J. W. McCaffrey, G. P. Roberts, P. A. Cowie, R. J. Phillips, A. M. Michetti, E.
743 Vittori, L. Guerrieri, A. M. Blumetti, A. Bubeck, A. Yates, and G. Sileo (2010),
744 Partitioned postseismic deformation associated with the 2009 Mw 6.3 L'Aquila
745 earthquake surface rupture measured using a terrestrial laser scanner, *Geophys.*
746 *Res. Lett.*, *37*(10), 1–7, doi:10.1029/2010GL043099.

747 Wilkinson, M., G. P. Roberts, K. J. W. McCaffrey, P. A. Cowie, J. P. Faure Walker, I. D.
748 Papanikolaou, R. J. Phillips, A. M. Michetti, E. Vittori, L. Gregory, L. Wedmore, and Z.
749 K. Watson (2015), Slip distributions on active normal faults measured from LiDAR
750 and field mapping of geomorphic offsets: an example from L'Aquila, Italy, and
751 implications for modelling seismic moment release, *Geomorphology*, *237*, 130–141,
752 doi:10.1016/j.geomorph.2014.04.026.

753 Zollo, A., S. Marcucci, G. Milana, and P. Capuano (1999), The 1997 Umbria-Marche
754 (central Italy) earthquake sequence: Insights on the mainshock ruptures from near
755 source strong motion records., *Geophys. Res. Lett.*, *26*, 3165–3168.

756 **Figure Captions**

757 Figure 1: Summary map of the studied region. Map shows the location of towns and the
758 active normal faults (red lines), ATR=Atri, CAS=Casci, CSM= Costa-San Martino,
759 GUB=Gubbio, GUT= Gualdo Tadino, GU2=Gubbio 2, LAG= Laga, LEO=Leonessa,
760 MAL= Mt. Alvagnano, MAR= Martana, MLS= Mt. Le Scalette, MSV=Mt. San Vicino,
761 MVT= Mt. Vettore, NOR= Norcia, TER= Terni, UMV= Umbra Valley. Lower
762 hemisphere focal mechanisms for the three mainshocks of the 1997 Umbria-
763 Marche seismic sequence are shown, black mechanisms are from the CMT

764 catalogue (*Dziewonski et al.*, 2003), blue mechanism is from *Cattaneo et al.*, 2000c.
765 Purple rectangle shows the extent of Figure 4. Inset shows the location of the main
766 map as a blue box within Italy.

767 Figure 2- Block diagrams illustrating the relationship between the strike, dip and throw
768 of a normal fault. (a) Simplified fault where the central section exhibits a bend. The
769 slip vector azimuth remains constant across the fault (black arrows). Adapted from
770 Figure 3, Faure Walker et al (2015). (b) The surface trace of the fault, with the
771 central bend labelled. Adapted from fig. 3, Faure Walker et al (2015). (c) Graphs
772 showing how the throw rate is expected to vary in the central section relative to
773 the main fault as the strike or dip are varied independently. The principal strain
774 rate is assumed to be constant across the fault trace. Adapted from Figure 6c and
775 7c, Faure Walker et al (2009). It is shown as the orientation of the central section
776 becomes more oblique to the slip vector or the dip increases, the relative throw
777 rate is expected to increase for a constant principal strain rate.

778

779 Figure 3: View of a section of the Mt Le Scalette fault scarp, close to the centre of the
780 large scale corrugation mapped in Figure 3. a.) Views along the bedrock scarp,
781 looking to the north-west. b.) view onto the bedrock scarp. White dashed box
782 shows the extent of c.)close up of the base of the bedrock scarp, note that there is a
783 fresh stripe at the base, which is also marked by the lack of moss growth
784 (especially to the left hand side of the photograph. The unweathered stripe at the
785 base of the scarp marked in a dashed red line.

786

787 Figure 4: Structural and geomorphic map of a well-exposed section close to the centre of

788 the Mt Le Scalette fault. Strike and dip data are grouped together over 20m
789 sections, the mean strike and dip are reported on the map and the corresponding
790 stereonets are shown. Kinematic indicators were found at four localities along the
791 section, the mean slip-vector plunge and azimuth are reported on the map and the
792 corresponding stereonets shown. The mean slip vector is 61 –> 211. The
793 topographic profile created from the TLS data gives the Holocene throw of the fault
794 and the Holocene throw rate is calculated from this. B – B' indicates the orientation
795 of the data plotted in Figure 5. The white dashed box around the profile line A-A'
796 indicates the extent of b.) hillshade DEM with 2m contours from a TLS survey. The
797 fault scarp and upper slope boundary are marked. The mean slip vector and
798 orientation of the upper and lower slope are marked. c.) frequency plot of the
799 aspect of the lower and upper slopes from the TLS data. The mean trend of the slip
800 vector measured from frictional wear striae on the fault plane does not align with
801 the direction of maximum slope.

802

803 Figure 5: All structural data collected and plotted against distance along the fault,
804 indicated by B – B' in Figure 3. a.) strike against distance, uncertainties are smaller
805 than the symbols, the black line is perpendicular to the mean trend, the grey
806 shaded region is the 95% confidence interval of the trend (calculated from
807 Stereonet). b.) dip against distance, uncertainties are smaller than the symbols, the
808 black line is the mean plunge, the grey shaded region is the 95% confidence
809 interval of the trend. c.) vertical height of the unweathered stripe against distance.
810 d.) strike against dip, data points are mean strike and dip values for 20m sections
811 of the fault (see Figure 4) with 95% confidence interval plotted as the error. A

812 systematic relationship can be seen between the strike, dip and height of the stripe
813 from these diagrams.

814

815 Figure 6: Map and cross sections of different published locations for the three
816 mainshocks of the 1997 seismic sequence. a.) map view of the Colfiorito region
817 affected by the 1997 seismic sequence. The traces of active normal faults are
818 marked in red. Coloured circles refer to different published locations; (1) *Cello et*
819 *al.*, 1998, (2) INGV, *Castello et al.*, 2006, (3) *Boncio and Lavecchia*, 2000a, (4) *ISC*,
820 2012, (5) *Amato et al.*, 1998, (6) *Cocco et al.*, 2000, (7) *Cattaneo et al.*, 2000, (8)
821 *Chiarabba et al.*, 2009. Stereonets show the mean strike and dip for the two faults,
822 MLS=Mt Le Scalette fault, CSM= Costa-San Martino fault. b.) cross-section of Event
823 1, c.) cross-section of Event 2, d.) cross-section of Event3. Cross-sections show the
824 reported errors for each location, where published and the different reported dips
825 for each earthquake. The red line indicates mean measured dip of each fault,
826 projected to depth, with the 95% and 99% confidence intervals and full range of
827 measured dips. This demonstrates that when the range of locations and dips are
828 taken into account, there is overlap between the projected dip from the surface and
829 the locations of earthquakes at depth and hence the surface fault scarps should be
830 considered as active.

831

832 Figure 7: Comparing published dips of the three mainshocks to the dip of the surface
833 fault scarps (from field measurements). Dips at depth are calculated by different
834 methods and published by (1) *Ekström et al.*, 1998, (2) *Weston et al.*, 2011, (3)
835 *Cattaneo et al.*, 2000, (4) *Zollo et al.*, 1999, (5) *Chiaraluce et al.*, 2005. Field

836 measurements of the dip were measured from bedrock fault scarp by the authors
837 along the Mt Le Scalette and Costa-San Martino faults. For each event, there is an
838 overlap between the dip at depth (from the literature) and the dip of the surface
839 scarp. Hence, it cannot be argued that the surface scarps are inactive due to a
840 mismatch between dip at depth and dip at the surface.

841

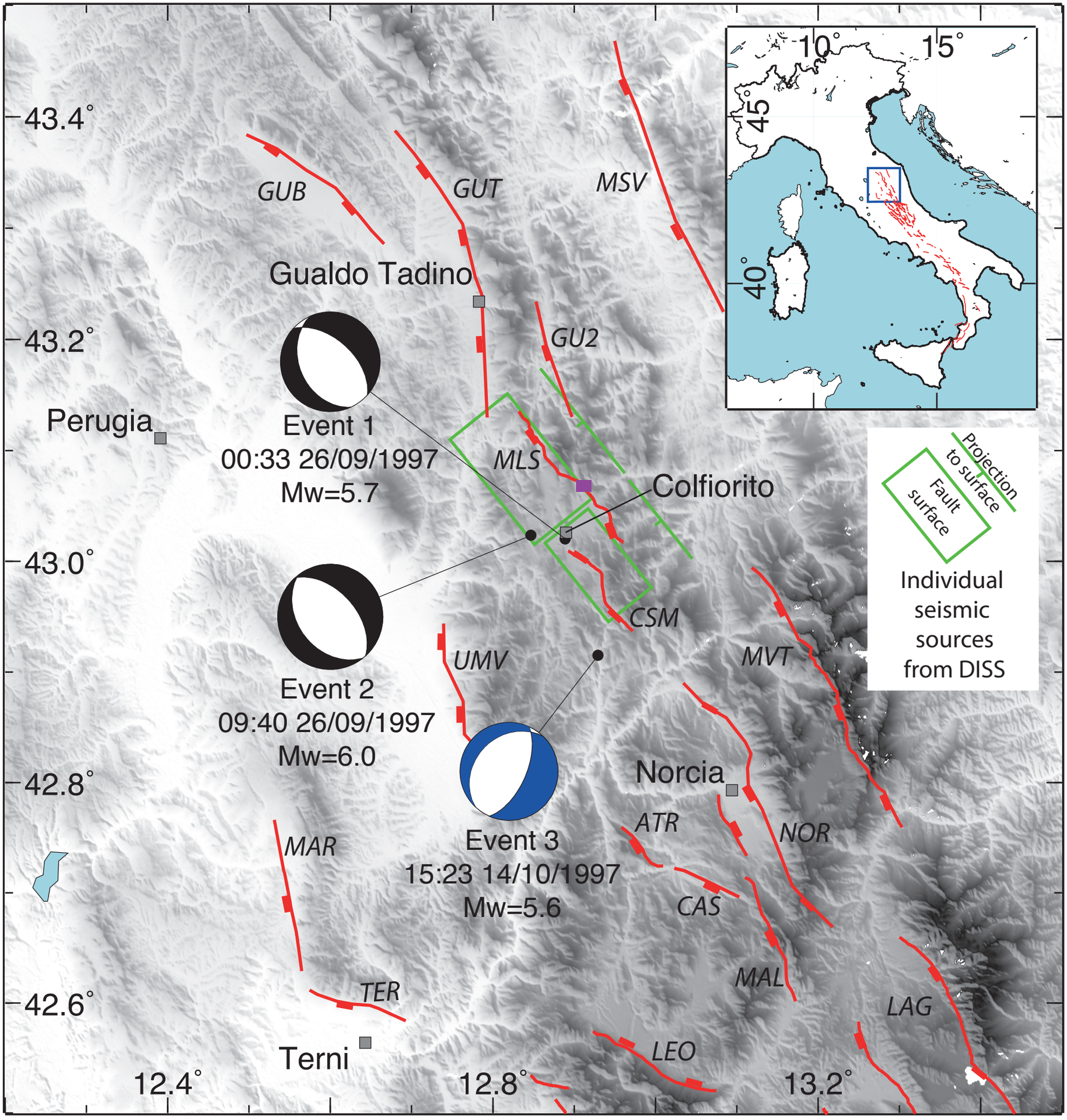
43.4°
43.2°
43.0°
42.8°
42.6°
12.4°
12.8°
13.2°
GUB
GUT
MSV
GU2
MLS
CSM
UMV
MVT
ATR
NOR
CAS
MAL
LAG
LEO
MAR
TER
Gualdo Tadino
Perugia
Colfiorito
Norcia
Terni
Event 1
00:33 26/09/1997
Mw=5.7
Event 2
09:40 26/09/1997
Mw=6.0
Event 3
15:23 14/10/1997
Mw=5.6
10°
15°
45°
40°
Projection to surface
Fault surface
Individual seismic sources from DISS

a. Block diagram of a fault with a central bend

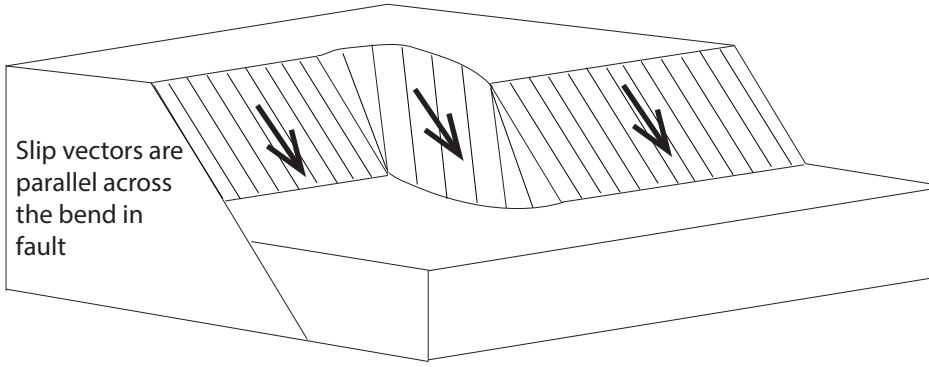

b. Surface trace of the fault with a central bend

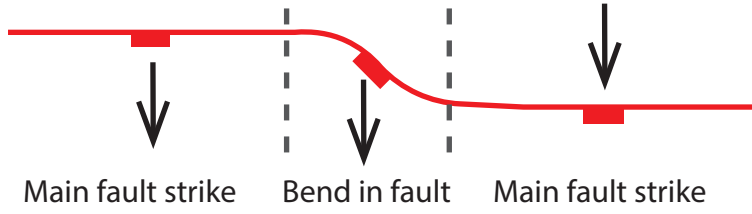

c. Effect on the throw rate as the strike or dip is varied

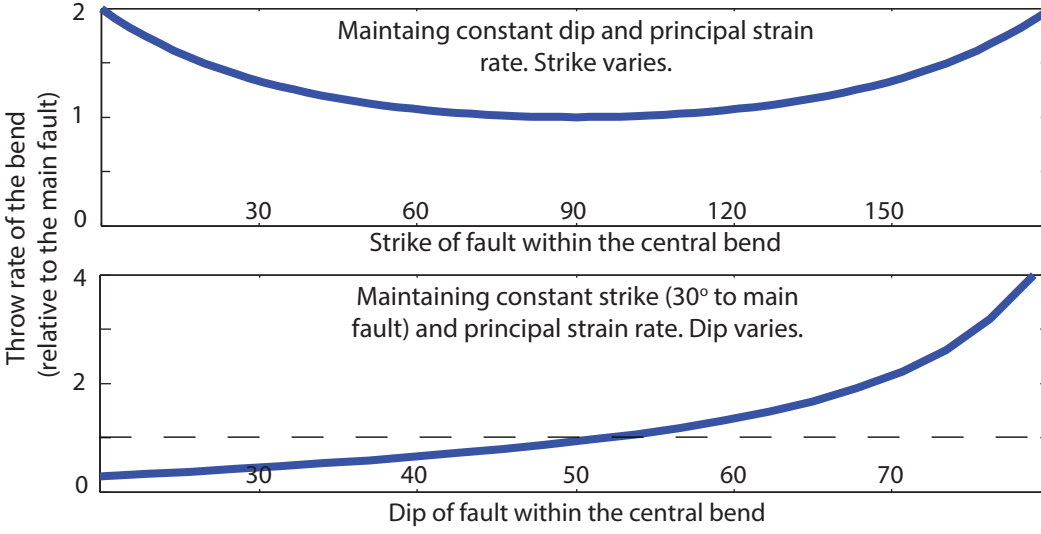

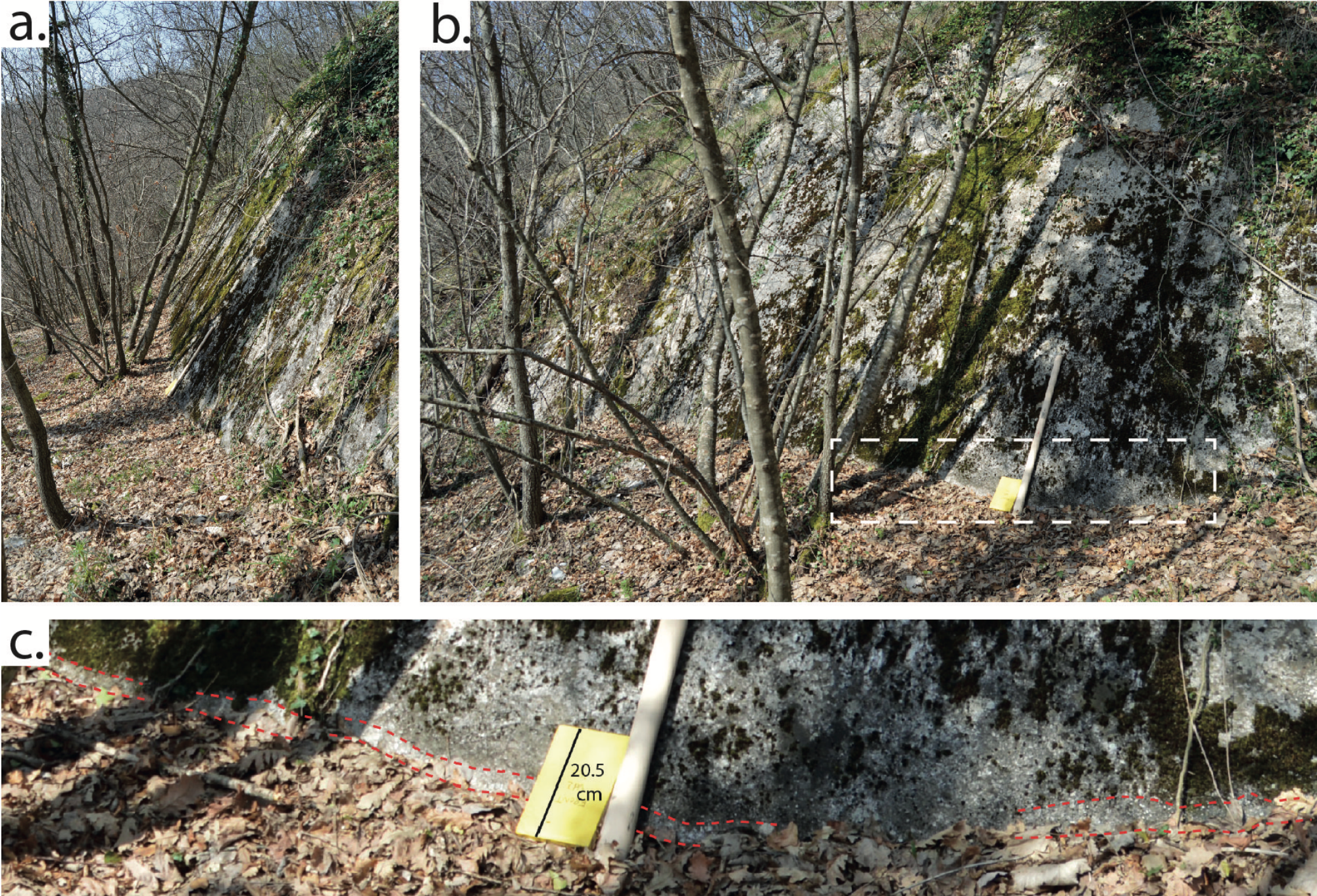
a.
b.
c.
20.5
cm

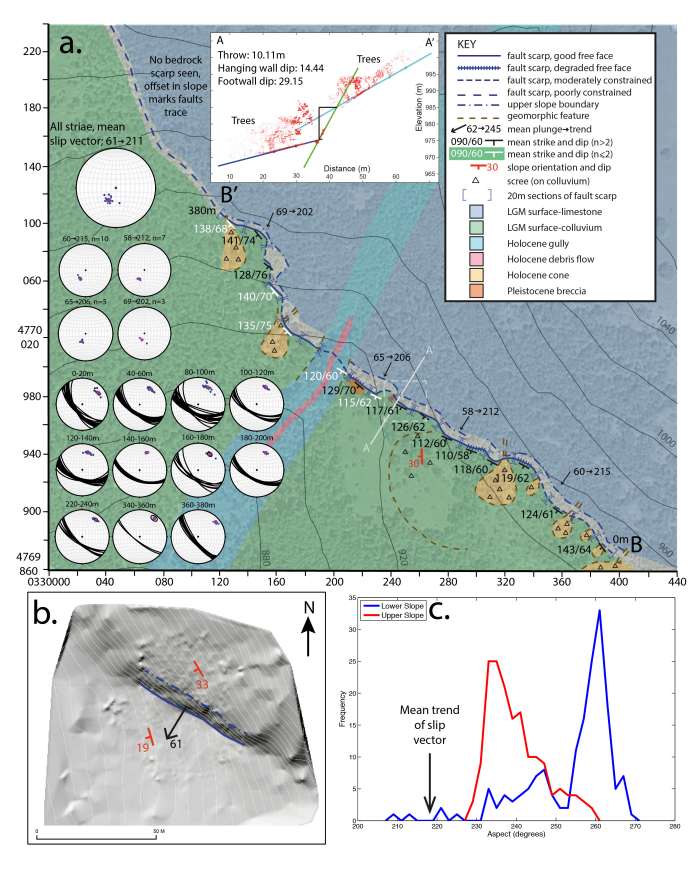
a.
No bedrock scarp seen, offset in slope marks faults trace
All striae, mean slip vector: 61→211
A
Throw: 10.11m
Hanging wall dip: 14.44
Footwall dip: 29.15
A'
Trees
Trees
Elevation (m)
Distance (m)
KEY
fault scarp, good free face
fault scarp, degraded free face
fault scarp, moderately constrained
fault scarp, poorly constrained
upper slope boundary
geomorphic feature
62→245 mean plunge→trend
090/60 mean strike and dip (n>2)
050/60 mean strike and dip (n<2)
30 slope orientation and dip
scree (on colluvium)
20m sections of fault scarp
LGM surface-limestone
LGM surface-colluvium
Holocene gully
Holocene debris flow
Holocene cone
Pleistocene breccia
B'
380m
69→202
138/68
141/74
128/76
140/70
135/75
65→206
120/60
129/70
115/62
117/61
126/62
112/60
110/58
118/60
58→212
30
19/62
124/61
60→215
143/64
0m
B
A'
A
60→215, n=10
58→212, n=7
65→206, n=5
69→202, n=3
0-20m
40-60m
80-100m
100-120m
120-140m
140-160m
160-180m
180-200m
220-240m
340-360m
360-380m
0330000
040
080
120
160
200
240
280
320
360
400
440
860
900
940
980
020
060
100
140
180
220
4769
4770
b.
N
33
19
61
0
50 M
c.
Lower Slope
Upper Slope
Mean trend of slip vector
Frequency
Aspect (degrees)

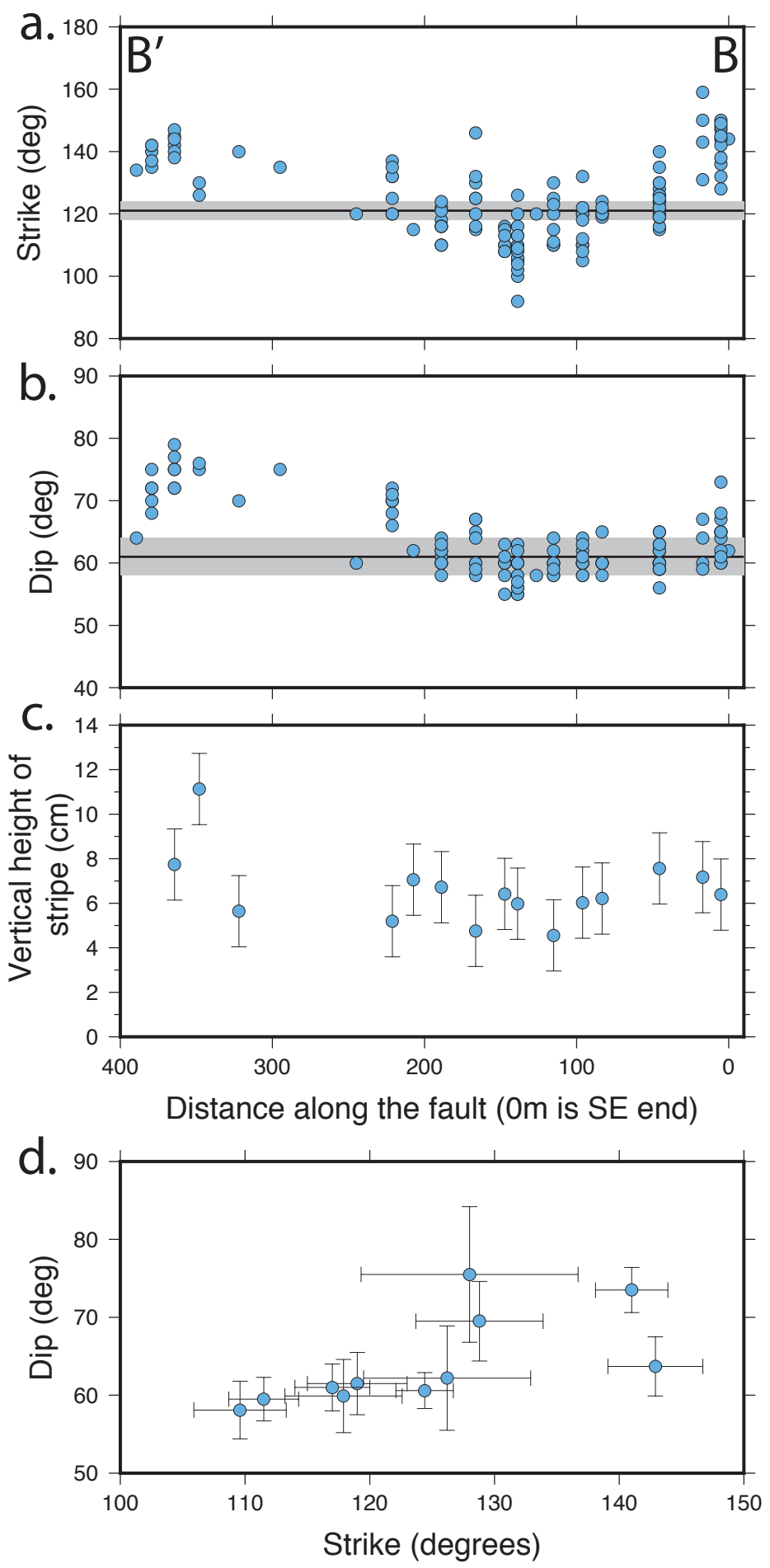
a.
B′
B
Strike (deg)
180
160
140
120
100
80
b.
Dip (deg)
90
80
70
60
50
40
c.
Vertical height of stripe (cm)
14
12
10
8
6
4
2
0
400
300
200
100
0
Distance along the fault (0m is SE end)
d.
Dip (deg)
90
80
70
60
50
100
110
120
130
140
150
Strike (degrees)

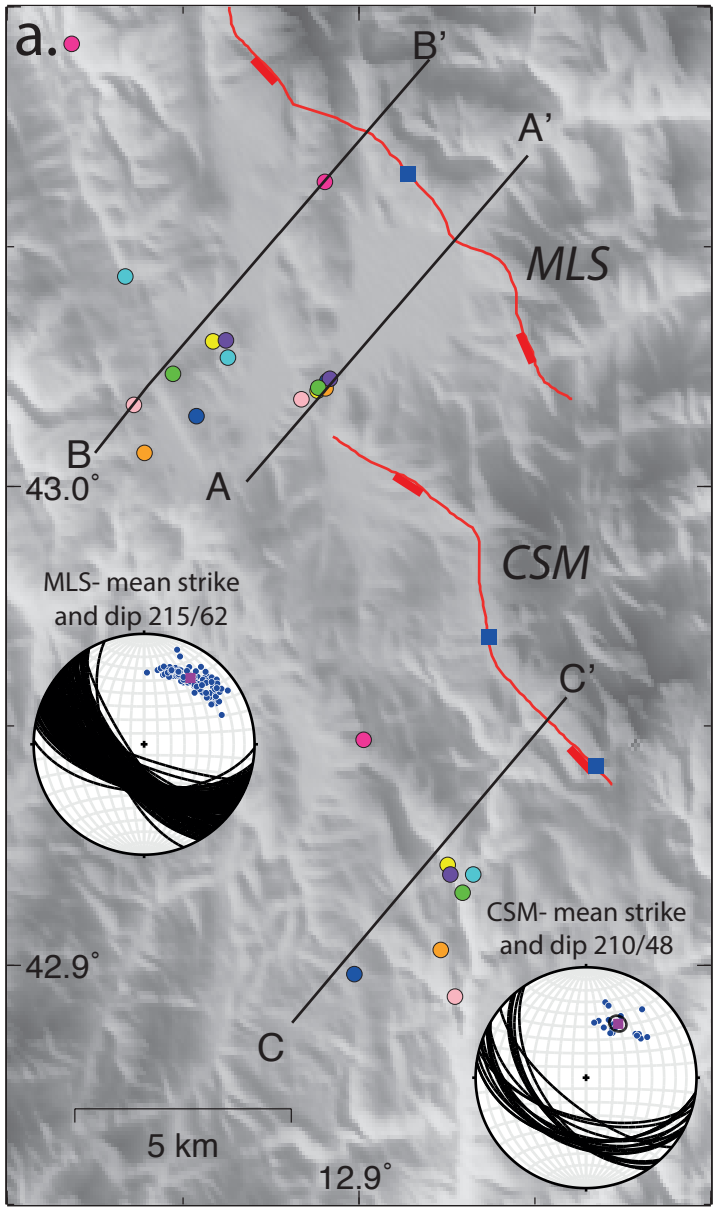

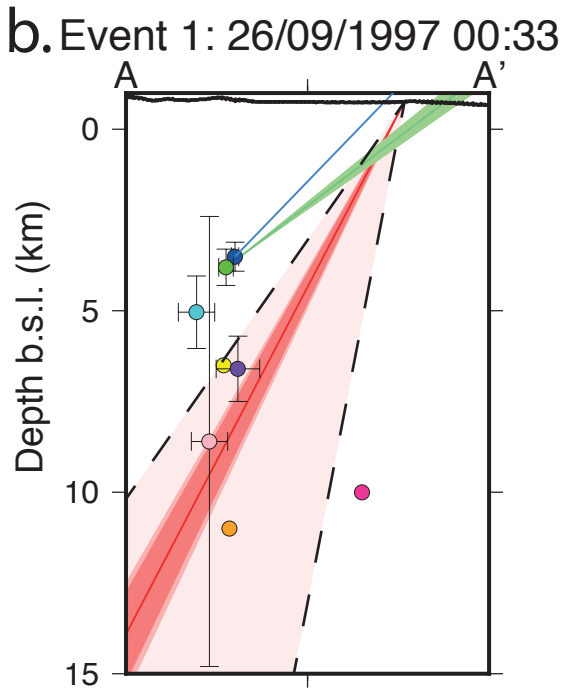

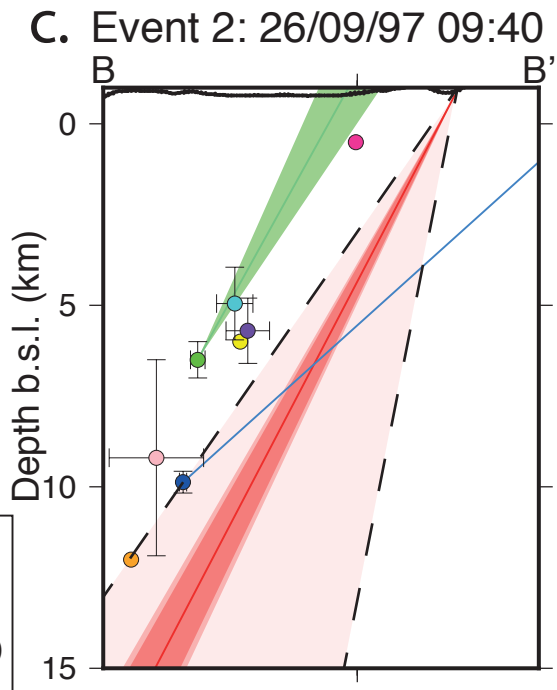

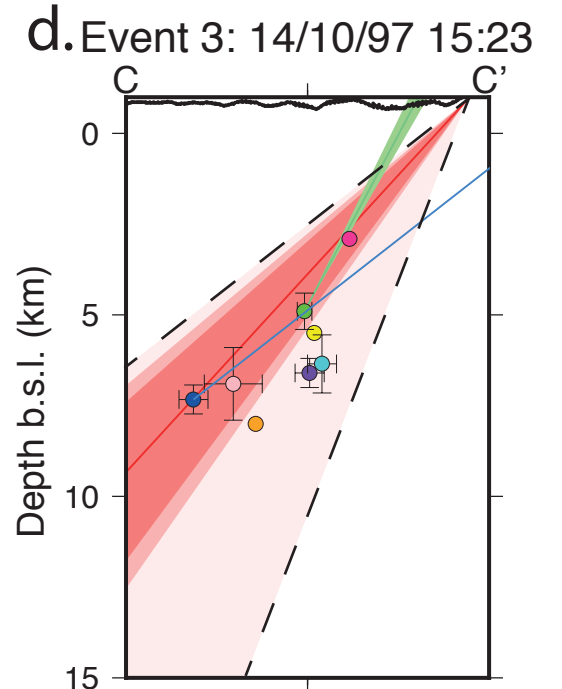

- Preliminary locations (1)
- National&regional network, 1D velocity model (INGV, 2)
- Temporary local network, 3D velocity model (XGUMS, 3)
- ISC location, teleseismic data (4)
- Local&ING network (5)
- Local network, 2D velocity model, HypoINVERSE (6)
- Local network, 3D velocity model (7)
- Local network, 3D velocity model, HypoDD (8)
- Surface expression of active normal faults
- Cross–section (perp to fault of interest)
- Dip from CMT catalogue (on INGV location)
- Dip from a local network (7)
- Dip error from a local network (7)
- Locations of field measurements
- Mean dip from field measurements
- 95% confidence interval of field measurements
- 99% confidence interval of field measurements
- Range of dip from field measurements

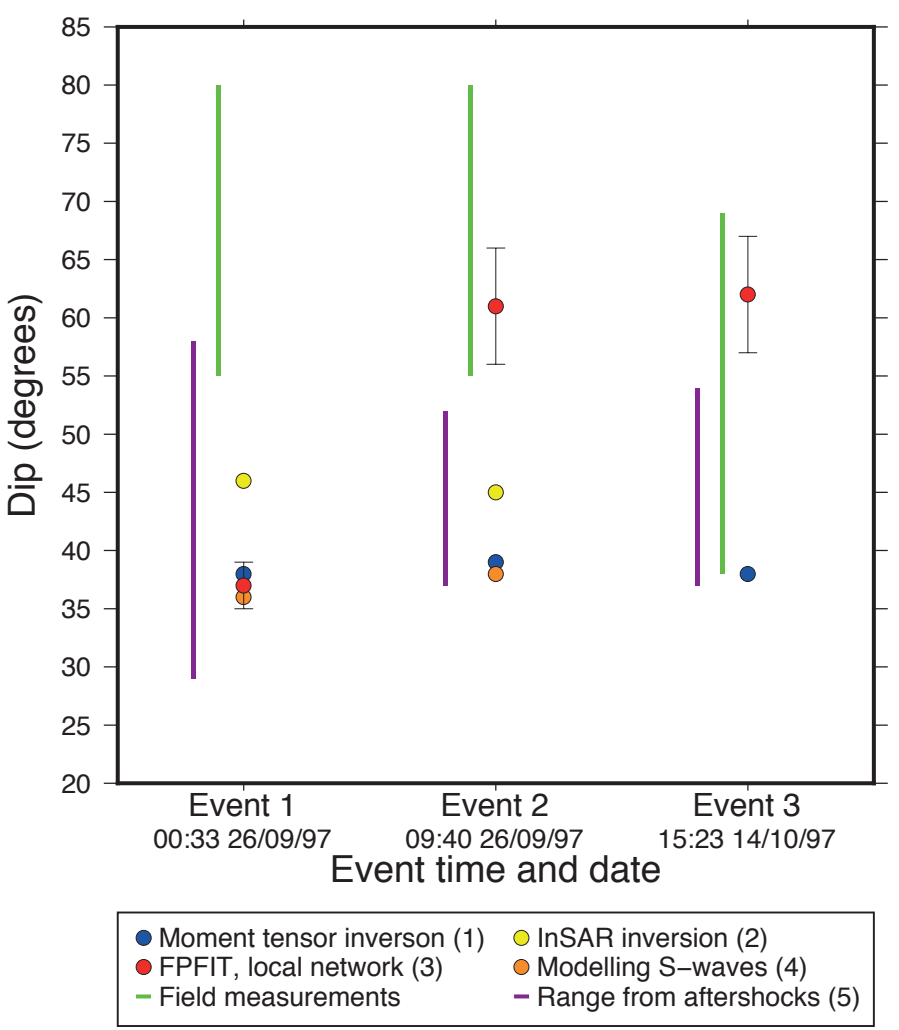
Dip (degrees)
85
80
75
70
65
60
55
50
45
40
35
30
25
20
Event 1
00:33 26/09/97
Event 2
09:40 26/09/97
Event 3
15:23 14/10/97
Event time and date
Moment tensor inverson (1)
InSAR inversion (2)
FPFIT, local network (3)
Modelling S–waves (4)
Field measurements
Range from aftershocks (5)